Studies of Transition Radiation Detectors for AMS

by

Bilge Melahat Demirköz

Submitted to the Department of Physics
in partial fulfillment of the requirements for the degree of

Bachelor of Science in Physics

at the

MASSACHUSETTS INSTITUTE OF TECHNOLOGY

June 2001

Author .....
Department of Physics
May 11, 2001

Certified by .....
Ulrich J. Becker
Professor, Department of Physics
Thesis Supervisor

Accepted by .....
David E. Pritchard
Senior Thesis Coordinator, Department of Physics

Studies of Transition Radiation Detectors for AMS

by

Bilge Melahat Demirköz

Submitted to the Department of Physics
on May 11, 2001, in partial fulfillment of the
requirements for the degree of
Bachelor of Science in Physics

Abstract

Detectable transition radiation is emitted by charged particles with a Lorentz factor greater than 1000. This allows one to distinguish between positrons, which radiate, from protons which do not, in the 0.3 to 300 GeV range measured by Alpha Magnetic Spectrometer(AMS-02). The detection and discrimination critically depends on the balance of creation and absorption of the transition radiation. The absorption properties of detector materials are measured and discussed.

Thesis Supervisor: Ulrich J. Becker
Title: Professor, Department of Physics

Acknowledgments

The author would like to thank Profs. Ulrich Becker, Peter Fisher and Kate Scholberg for their help and guidance through the research; Dr. Jay Kirsch and Scott Sewell and for letting me borrow Junior Lab equipment; Reyco Henning, Benjamin Monreal and Josh Thompson for their help and support. The author also thanks Drs. Thomas Kirn and Thorsten Siedenburg of RWTH, Aachen for providing the preamplifier design.

Contents

List of Figures

List of Tables

Chapter 1

Introduction

Transition radiation detectors are proportional counters which detect the radiation emitted when a charged high energy particle passes through the interface between two media with different dielectric constants. This radiation was first predicted in 1946 by Ginzburg and Frank. However, it was not studied experimentally for a long time since the expected number of quanta produced was low. It was first observed in the optical region. Later, Garibian showed that the radiation was in the X-ray region for ultra-relativistic particles and that the intensity was proportional to the Lorentz γ factor. [14] Hence the TRD is very useful for distinguishing ultra-relativistic particles where other methods of determining the velocity become ineffective; for example in discriminating between a 50 GeV electron and a 50 GeV proton; since electrons emit measurable TR photons above 0.5 GeV and protons above 1000 GeV.

Such a detector allowing good particle discrimination is ideal for use in the Alpha Magnetic Spectrometer (AMS). AMS is a high energy physics experiment with high resolution detectors that will be installed on the International Space Station in 2003. The aim of this experiment is to find antimatter in space, look for evidence for supersymmetric particles through the positron and the antiproton spectrum and to obtain the cosmic ray spectra in the range of 0.3 GeV to 3 TeV. From AMS-01 and balloon experiments, the cosmic ray flux at low earth orbit mostly consist of high energy protons, leptons, He and anti-protons. [2, 3, 22] Hence it is very important to have a good discrimination between protons and positrons and the AMS TRD should

provide a rejection factor of 10^{-2}-10^{-3} of protons from positrons.

This thesis will first present the theory and briefly discuss the optimization of the TRD and give examples of their usage in high energy particle physics in Chapter 1. In Chapter 2, the physics of the AMS TRD is discussed with focus on the attenuation of the TR X-rays and some results are quoted from experiments which have used TRDs. In Chapter 3, gain measurements with different gas mixtures and different X-ray energies are presented. The measurements of attenuation constants also for different X-ray energies are compared to theoretical calculations from the National Institute of Standards and Technology (NIST). [17] Then the effect of attenuation on the TRD spectrum and total energy deposition in the tubes is shown. Finally, the effects of attenuation on the positron-proton separation and the implications on the physics results are discussed in the conclusion.

Chapter 2

Transition Radiation

2.1 Theory

Transition radiation is electromagnetic radiation that is emitted when a uniformly moving charged particle traverses the boundary between two media with different dielectric constants, ϵ_1 and ϵ_2. Far away from the boundary, the particle induces fields that are defined by the particle's motion and the characteristics of that medium, such as ϵ_1. Later, when it is the second medium, it has fields that are defined by the properties of that medium and its motion in that medium. Although the motion is uniform, the fields are still different in each media. As the particle is approaching and leaving the interface between the media, the fields have to reorganize to compensate for the change and some part of this compensation is radiated off as the "transition radiation."

2.1.1 Production of Transition Radiation

The transition radiation intensity can be expressed as [14]

$$\frac{dW}{d\omega d\theta} = \frac{2\alpha}{\pi}\theta^3 \left(\frac{1}{\gamma^{-2} + \theta^2 + (\omega_1/\omega)^2} - \frac{1}{\gamma^{-2} + \theta^2 + (\omega_2/\omega)^2} \right)^2 \tag{2.1}$$

where γ is the Lorentz factor, θ is the angle at which the radiation is emitted with respect to the trajectory of the particle, α is the fine structure constant, ω is the

energy of the radiated photon, and w_1 and w_2 are the plasma frequencies of the initial and final medium, respectively. Using $\epsilon_i = 1 - \frac{\omega_i^2}{\omega^2}$ and integrating over the the angles θ gives

$$\frac{dW}{d\omega} = \frac{\alpha}{\pi}\left(\frac{\epsilon_2^2 + \epsilon_1^2 + 2\gamma^{-2}}{(\omega_2/\omega)^2 - (\omega_1/\omega)^2} ln \frac{\gamma^{-2} + \epsilon_2^2}{\gamma^{-2} + \epsilon_1^2} - 2\right). \tag{2.2}$$

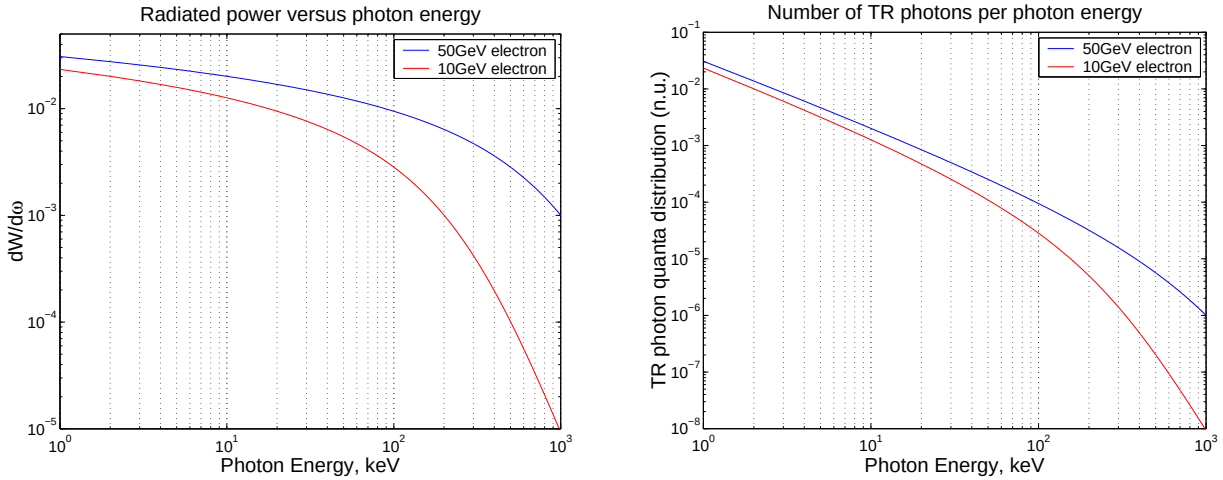

(a) (b)

Figure 2-1: a) Radiated power distribution for photon energies, b) Number of TR photons radiated per photon energy (not normalized). Calculations were done using Eq. 2.1 and 2.2 for transitions from vacuum to polyethylene.

Assuming that the initial medium is vacuum, the total energy emitted in transition radiation per interface is approximately [18]

$$I = \frac{z^2\hbar}{3}\alpha\gamma w_r \tag{2.3}$$

where ω_r is the plasma frequency of the radiator and z is the charge of the particle.

There are several features and considerations that need to be highlighted in the optimal design of a TRD.

1. The radiation is proportional to the Lorentz factor, γ as seen from Eq. 2.3. Detectors built on this principle are ideal for use in the ultra-relativistic region

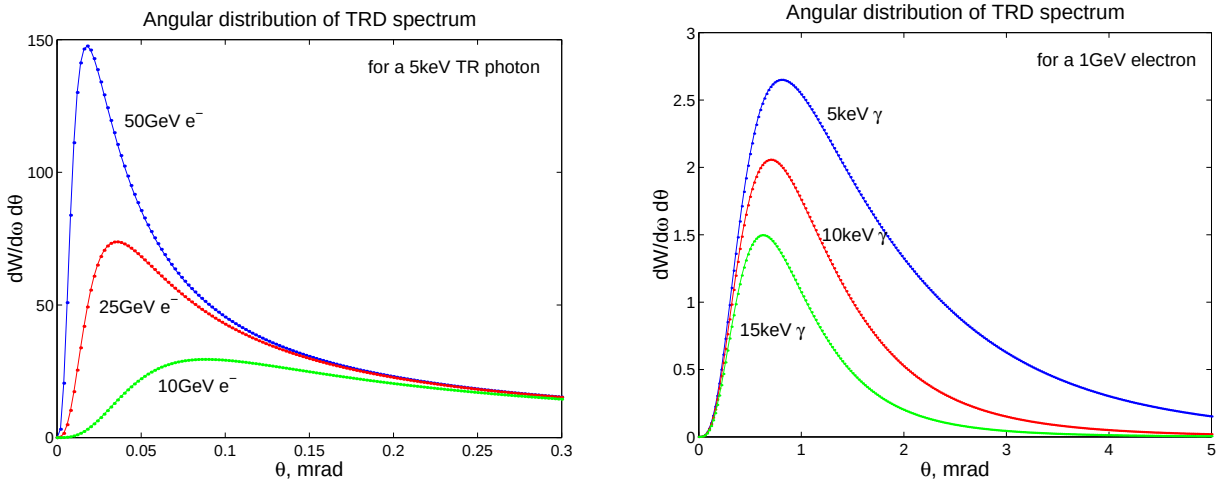

(a) (b)

Figure 2-2: The angular distribution of TR with a) different γs and b) different TR photon energies.

where other detectors become ineffective. Detectors with sensitivity to β, such as the Cerenkov, time of flight, and silicon detectors in the ultra-relativistic region can not provide a good resolution of the energy of the particle; particle discrimination fails in any measurement involving ionization loss.

2. The number of emitted TR photons falls exponentially with the photon energy as seen on Fig. 2-1(b). Depending on the characteristics of the radiator, the spectrum of radiation is mostly in the X-ray region. For example, most of the TR quanta for a 50 GeV electron are emitted below 20 keV. However, there is a cutoff to the lower end of this spectrum, that will be discussed later, due to attenuation of low energy X-rays. This demands that the walls of the proportional counter has to be thin enough to be transparent to most of the X-rays.

3. The probability of creating a TR photon per layer of interface in the radiator is low; on the order of the fine structure constant, $\alpha \approx 1/137$. However, stacking a large number of interfaces of thin radiator material can enhance the TR photon production. On the other hand, there is a compromise since increasing the

number of material also increases the absorption. This will be discussed again later.

4. Most of the TR photon emission is strongly peaked in the forward direction, within the cone of half angle $1/\gamma$, as can be obtained from Eq. 2.1 and can be seen in Fig. 2-2(a). This implies that the ionization energy loss of the particle will be deposited in the detector, as well as the transition radiation component, unless a separation of the particle from the radiation is forced by a magnetic field. In general, such a separation is not necessary if the energy loss of the particle in the medium, dE/dx, governed by the Bethe-Bloch formula is well understood and simulated.

These considerations put emphasis on the following points in the design of an optimal TRD:

- Material of the TR radiators: The plasma frequency of radiators can vary from 0.7 eV(air) up to 33 eV (aluminum) and this determines how hard the TR spectrum is.

- Characteristics of the TR detection system: The gas composition and high voltage of proportional counters determines the response of the detectors, hence the sensitivity to the TRD spectrum.

- Thickness of the materials: The absorption of X-rays, between the point they are produced in the radiator to the point in the detector where they are detected, changes the TRD spectrum. It is important to understand and quantify the effect of attenuation due to the materials.

The choice of TR radiator is beyond the scope of this thesis, however, the response of the detector with gas composition and high voltage will be discussed as well as the attenuation due to the materials.

The effectiveness of a TRD system is quantified in terms of a "rejection factor," $\mathcal{R}$, and an efficiency percent, $\mathcal{E}\%$. Say we want to choose cuts that will discriminate between protons and positrons. $\mathcal{R}$ is defined as the fraction of misidentified protons

Particle	Abundance
Protons	1.0
Helium and heavier elements	0.15
Electrons	0.02
Positrons	0.002
Antiprotons	$1 * 10^{-4}$

Table 2.1: Approximate abundances of cosmic rays normalized to proton flux.

in the positron sample. $\mathcal{E}\%$ is the fraction of real positrons that pass the cut. The likelihood, $\mathcal{L}$, for identifying a positron observed with deposited energy E_i in the i^{th} TRD layer, is defined as

$$\mathcal{L}_| = \sum_{i=1}^{N} log \frac{P(E_i|e)}{P(E_i|p)} \tag{2.4}$$

where $P(E_i|e)$ is the probability that such an energy deposition would be observed from a positron and $P(E_i|p)$ is likewise for protons. The rejection gets better as more and more layers are added. When the cut of $\mathcal{E}\%$ efficiency is defined on the positron likelihood function, it gives us a rejection factor for protons and vice versa. To achieve the physics goals of AMS with the cosmic ray abundances shown in Table 2.1, the TRD will be used in conjunction with the electromagnetic calorimeter to discriminate between protons and positrons. For the TRD, a rejection factor of $10^{-2} - 10^{-3}$ at $90 - 95\%$ efficiency is needed.

2.1.2 Detection of Transition Radiation

Straw proportional chambers are ideal for detection of the transition radiation since thin straw walls can minimize the attenuation of the X-rays. Also, the straw in each tube is at ground, avoiding noise pick-up. Any malfunction in one straw will be localized and therefore isolated from the rest of the detector. [23]

The radiation ionizes the gas mixture in the drift tube through the photoelectric process.[16] The number of ion-electron pairs formed will be the energy of the X-ray divided by the mean energy needed to create such pairs. For example, for a 5.9 keV

^{55}Fe source and Xe gas, which has a pair creation mean energy of 22 eV, the number of ion-electron pairs is 268. These electrons drift towards the wire due to the electric field they feel:

$$E = \frac{\lambda}{2\pi\epsilon_0}\frac{1}{r} \tag{2.5}$$

When the electron gets closer to the high-voltage wire and the electric field is large, the electron can pick up enough energy to ionize another gas atom, resulting in two electrons drifting. The primary electron signal is amplified by this avalanching process towards the high-voltage wire. For avalanche multiplications of $10^2 - 10^4$, the signal pulse is proportional to the initial number of electrons produced. But, the actual signal is formed by the induction due to the movement of ions and electrons as they drift towards the cathode and the signal wire. [19] Gain is the ratio of the detected number of electrons to the initial number of electrons produced.

It is important to operate drift chambers in the proportional region since the behavior of gain there is well understood: gain is an exponential function of the high voltage on the wire. This proportionality is possible since the voltage on the wire is uneffected by the deposition of the shower of electrons. The AMS TRD is optimized to operate in the proportional regime and with a gain of 5000. In this region, the gain can be approximated by the Diethorn formula. [11]:

$$lnG = \frac{Vln2}{ln\left(\frac{b}{a}\right)\Delta V} ln\left[\frac{V}{ln\left(\frac{b}{a}\right) aE_{min}(\rho)\left(\frac{\rho}{\rho_o}\right)}\right]. \tag{2.6}$$

The choice of gas in the straw tube is also important. A large signal out of the detector calls for a gas with a high stopping power for TRD quanta, which increases with density. Also, the low mean energy for ion-electron pair creation implies the low field intensities for avalanche formation. Noble gases are best in this aspect. Xenon, being the heaviest and easy to handle noble gas is the best choice. But, a quencher is needed to avoid UV feedback. UV radiation is produced by transitions within an ionized Xe atom. This radiation can contaminate the signal and to avoid

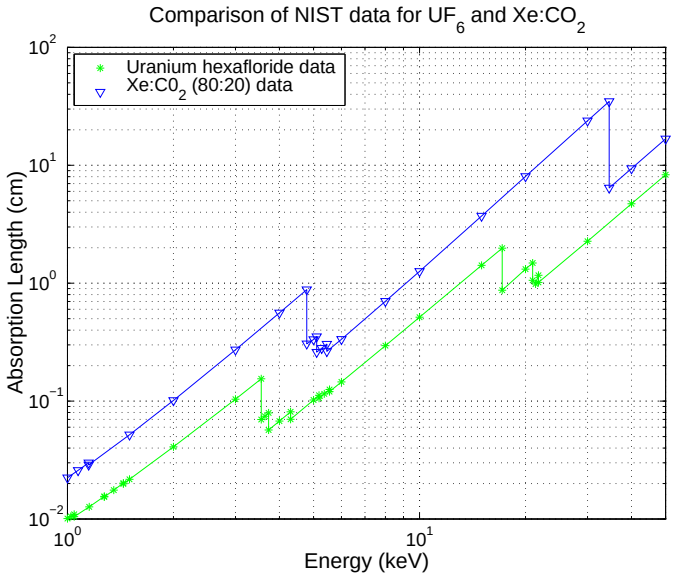

Figure 2-3: Comparison of stopping power of $Xe:CO_2 = (80:20)$ and UF_6.

this, quenchers that absorb UV radiation are needed. For the AMS TRD, a 20% gas volume of a quencher such as CO_2 or CF_4 is going to be used.

UF_6 would have been an ideal due to its higher stopping power if it was not corrosive and radioactive. In Fig. 2-3, it is compared with $Xe:CO_2 = 80:20$ where absorption length is the length of gas needed to stop $1/e$ of the photons and shorter absorption length implies larger stopping power.

2.2 Other Applications

Several experiments have used or proposed to use TRDs. Table 2.2 shows a list of such recent applications.

Experiment	**Use of TRD**	**Parameters**
NOMAD[8]	π and e separation for ν_μ oscillations	10^3 π rejection for 90% e efficiency
MACRO[20, 4]	energy spectrum of underground μ	sys. error $< 5\%$
HERA-B[23]†	tagging $B^0 \to J/\psi$, K_s^0	a) $> 95\%$ e efficiency b) hadron rejection from π up to 10^{-2}
D0[21]	top decay, $W \to e\nu$	5 fold hadronic rejection for 90% e eff.
E799[15]	Fermilab exp. on kaon decays	π/e rejection $> 120:1$
ATLAS[1]†	LHC experiment	still in R&D stage
WIZARD[10, 5, 6]	Balloon borne cosmic ray exp.	p and e rejection of 10^{-3}
BESS[22]	Balloon borne cosmic ray exp.	sys. error $< \pm 5\%$ for p and $< \pm 10\%$ for He
PAMELA[12]†	satellite born magnetic spectrometer	rejection p from $e^+ > 10^5$
AMS[7]†	Magnetic spectrometer on ISS	rejection factor of 10^{-2}-10^{-3} of p from e^+

Table 2.2: Some experiments with TRDs. (†) indicates proposed experiments.

Chapter 3

TRD for AMS

AMS is a high energy physics experiment with high resolution detectors that will be installed on the International Space Station in 2003 and will be operational for more than three years. AMS-01 was flown on the shuttle flight to MIR on STS-91 in June 1998 and collected data for seven days. The acceptances of AMS-01 are reported below in Fig. 3.1 along with the AMS-02 predictions. [3, 2, 7] AMS-01 did not have a TRD and the positron identification was performed by the aerogel Cerenkov detector which provides a p/e^+ separation only up to 3 GeV. (cf. Chapter 5)

The AMS TRD is optimized for positron proton separation. Although earlier versions of the TRD design had 2 dimensional tracking, this was later simplified since the cost would be too high. Immediately below the TRD is a Time of Flight(TOF) detector, followed by a magnetic spectrometer with silicon detectors, surrounded by a ACC, then another layer of TOF and a Ring Imaging Cerenkov detector and an

Experiment	**Particle**	P_{min} [GeV]	P_{max} [GeV]
AMS-01	Proton	0.1	200
	Electron	0.2	40
	Positron	0.2	3
AMS-02	Proton	0.3	3000
	Electron	0.3	3000
	Positron	0.3	300

Table 3.1: AMS acceptances for protons and leptons.

Material	Thickness
Kapton	50.0 μm
Carbon Polymide	12.0 μm
Polyurethene	10.0 μm
Aluminum	0.4 μm
Total	72.4 μm

Table 3.2: Straw tube composition.

electromagnetic calorimeter (ECAL). Most of the tracking will be done with the silicon detector and these tracks will be matched to hits in the TRD and others. While the tracker measures momentum, TOF determine the direction of the particle and the velocity and the RICH, the ECAL and the TRD are mainly for particle identification.

The transition radiation of interest to AMS is produced in the X-ray region of the spectrum(1-15 keV). The total energy loss includes the ionization losses of the charged particle. The sum is detected using proportional gas drift tubes.

The design of the TRD was done at RWTH Aachen and it includes:

- New high efficiency radiator made of polypropylene: fibers instead of foils. Fibers of thickness 10μm and density 0.06 gr/cm^3.
- Straw tubes of 6mm made out of complicated structure of 70μm wall thickness, seen in Table 3.2 and of length 1.5 to 2.2m.
- Gold-plated tungsten wires of diameter 60μm.
- Xe:CO_2 or Xe:CF_4 =80:20 gas supply from 8100 l of Xe and 2000 l of quencher. Either of these gases are good for AMS purposes as seen in Fig. 3-1.

To understand the detector better, a simulation is being written in GEANT, a simulation package. [13] The simulation takes every particle and tracks it through small incremenets in the detector materials; determines energy loss at every step and stoicastically allows for all known particle decays and interactions. The program has libraries containing constants of physical processes such as cross sections, decay rates and branching ratios. However, the transition photon generation had to be added to this package. While the X-ray attenuation constants are already in the program

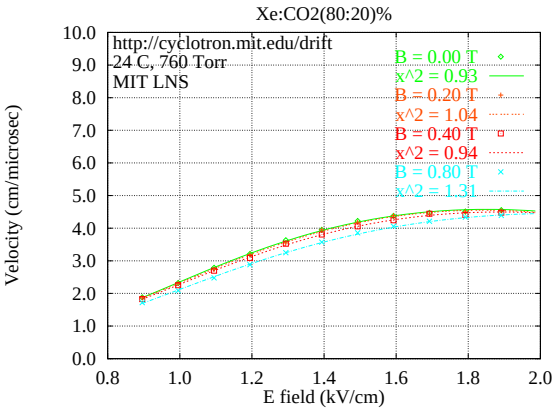

(a) Drift velocity vs. electric field for $Xe:CO_2$.

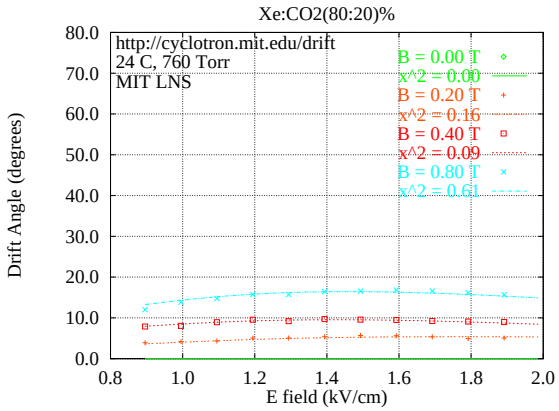

(b) Drift angle vs. electric field for $Xe:CO_2$.

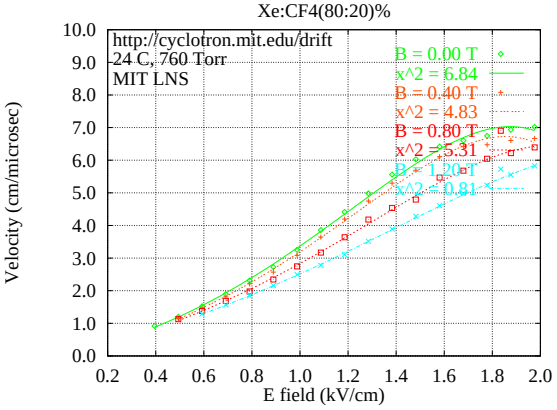

(c) Drift velocity vs. electric field for $Xe:CF_4$.

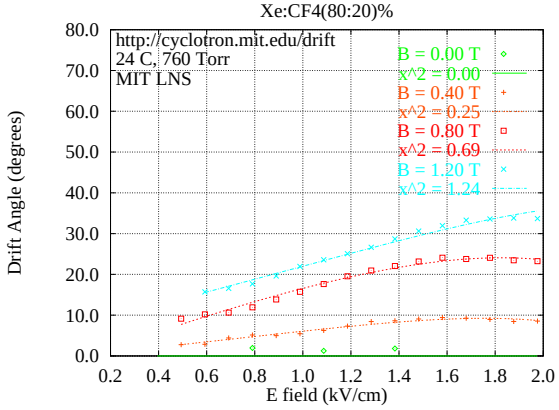

(d) Drift angle vs. electric field for $Xe:CF_4$.

Figure 3-1: $Xe:CF_4$ and $Xe:CO_2$ data from the Drift Gas R&D webpage. [9]

libraries, constants specific to the materials used in the TRD, had to be measured to compare to the calculated values and to attain better accuracy.

Chapter 4

Measurements

A 16 straw module similar to the one in the AMS TRD, produced at the Institute I of RWTH Aachen in Germany for the AMS collaboration was used. (Fig. 4-1) Gain and attenuation measurements are presented.

4.1 Experimental Setup

The system shown in Fig. 4-2 was flushed for 20 volume exchanges at a flow rate at 40 ml/minute. One volume was calculated to be 200 cm^3. The gain was checked for stability before measurements were taken. For all measurements, the same straw tube channel (channel #9) was used and cross-checked for stability with another channel, (channel #2).

The central wire of the straw tube is at high voltage. The signal wire is AC-coupled a capacitor in the preamplifier as seen in Fig. 4-3. The MCA and the preamplifier together were calibrated versus the input voltage using the 2.2pF test input of the preamplifier. This calibration was used in calculating the gain from the MCA channel.

X-rays and gamma-rays of known energy shown in Table. 4.1 were used. These radioactive X-ray sources were placed right above the straw tubes. ^{244}Po source is a 5.4 Mev α emitter. A thin foil of metal is placed on top of the source and X-rays, characteristic to the metals are back scattered. Titanium and silver metal foils were used to produce the 5.0 and 3.0 keV X-rays.

Source	Energy
^{210}Po: Ag-line	3.0 keV
^{210}Po: Ti-line	5.0 keV
^{55}Fe	5.9 keV
^{64}Co	6.4 keV
^{64}Co	14.4 keV

Table 4.1: Various radioactive sources with different energy X-rays.

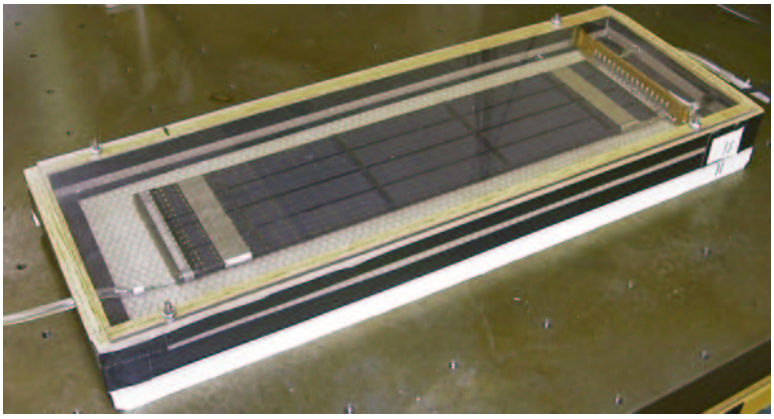

Figure 4-1: The experimental setup: the TRD module.

4.2 Detector Gases and Gain

A variety of gas mixtures tested in the TRD include Xe, Kr and Ar mixtures with 20% additions of CO_2 and CF_4. X-ray sources were used to test the output of

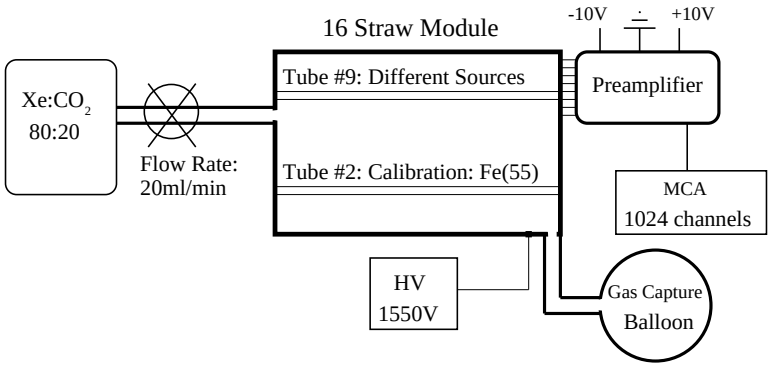

Figure 4-2: The experimental setup, with the TRD module, using different sources.

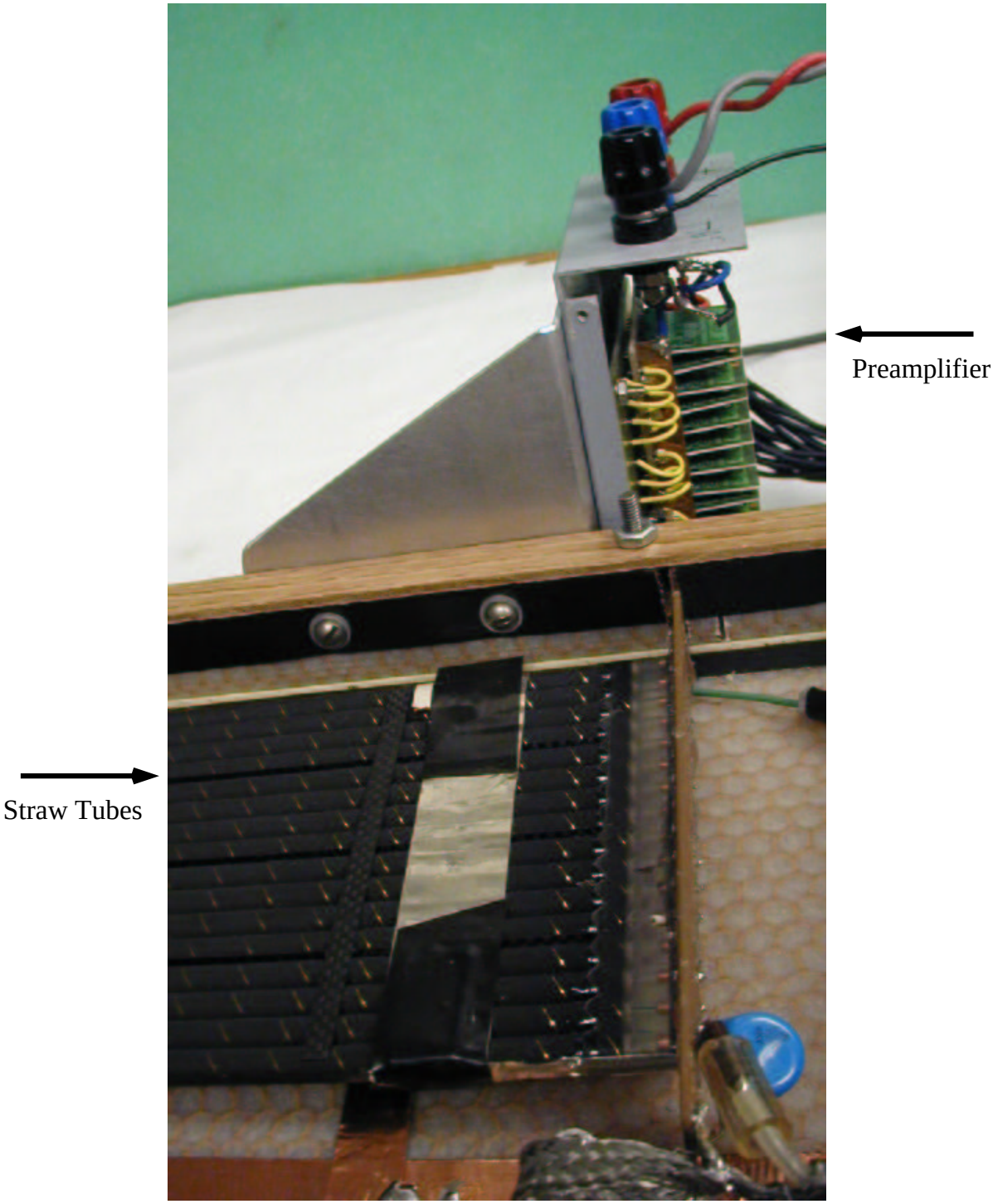

Figure 4-3: The experimental setup: the TRD module and the electronic readout.

the detectors to confirm the proportionality between the energy of the X-ray and the response of the detector. The signal charge distribution of different sources are shown in Fig. 4-4.

The gain measurements as a function of voltage with various X-ray energies with Xe:CO_2 = 80 : 20 are shown on Fig. 4-5. Pulse height measurements were normalized to the ^{57}Fe gain, by assuming 268 "primaries" for Xe gas with 5.9 keV X-ray. (cf. Chapter 2.1.2) It is important to note that the gain increases exponentially with high voltage as expected. Log(Gain) curves versus the pulse height measurements are all parallel as shown in Fig. 4-5(a). From this measurement, the average value for $\frac{1}{G}\frac{dG}{dV}$ is determined to be $1.00 \pm 0.02\%$.

However, gain plots for various X-ray energies do not all fall on top of one another when normalized with the number of primaries each source would produce as in Fig. 4-5(c). This could be either because there is a problem with energy calibration of the MCA or because the number of primaries do not scale linearly with the X-ray energy.

The gain measurements with Xe:CF_4 = 80 : 20 are shown on Fig. 4-6. One of the straw tubes sparked at 1615V with this gas and this straw tube was disconnected. However, other tubes started sparking at 1625V. Gain measurements were not taken past 1620V for this reason. Upon switching the gas and flushing the system with Xe:CO_2, such sparking problems went away.

For Xe:CF_4 = 80 : 20, the gain measurements for various X-ray energies do not all lie parallel as in Fig. 4-5(a). This problem was investigated several times. The temperature and pressure fluctuations were taken into account, however did not yield any significant change. The problem is not well understood at the present time. The average value for $\frac{1}{G}\frac{dG}{dV}$ for Xe:CF_4 = 80 : 20 was found to be $1.28 \pm 0.08\%$. Although this study has found some problems with Xe:CF_4, both gases are good for this purpose. The AMS TRD will be operated at a gain of 3000 to 5000 corresponding to a high voltage range of 1550 to 1600.

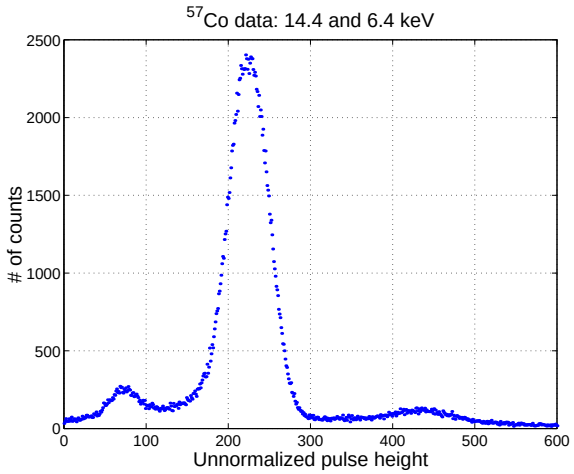

(a) ^{57}Co

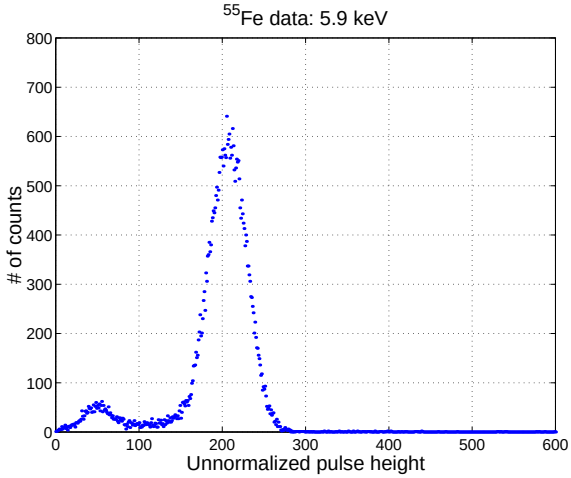

(b) ^{55}Fe.

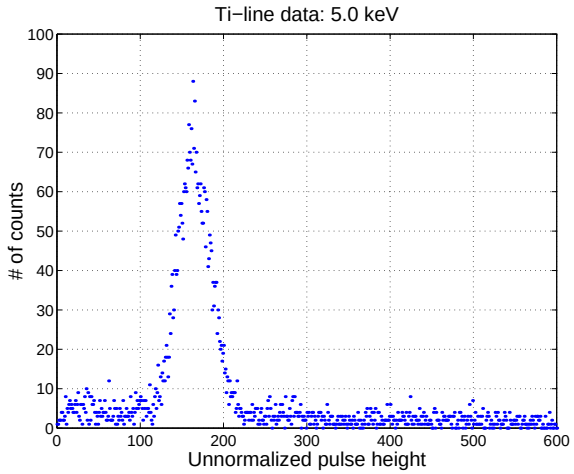

(c) Ti

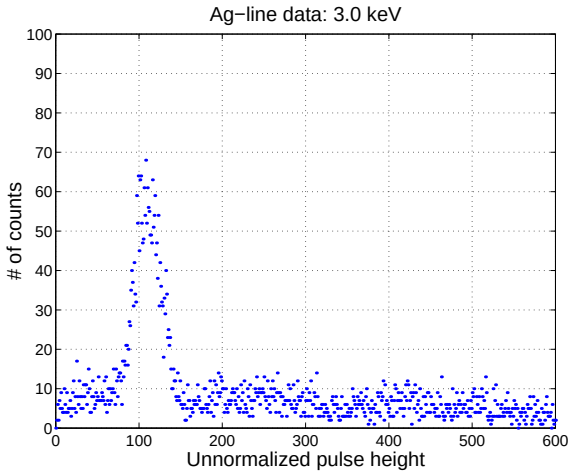

(d) Ag

Figure 4-4: Signal charge distributions for different X-ray sources with Xe:CO_2 at 1600V.

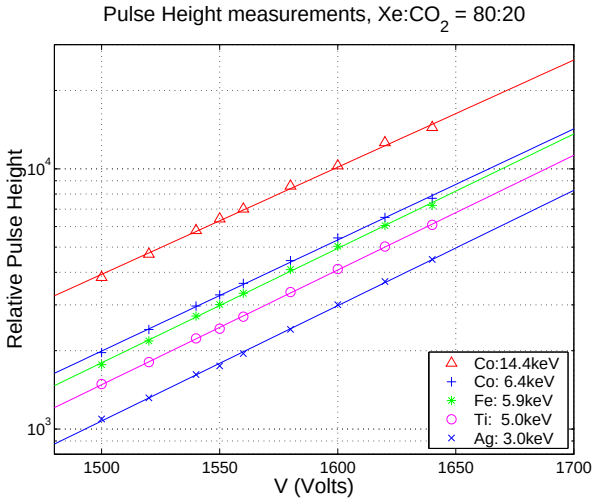

(a) Pulse height measurements vs. high voltage. Gain normalized to ^{55}Fe.

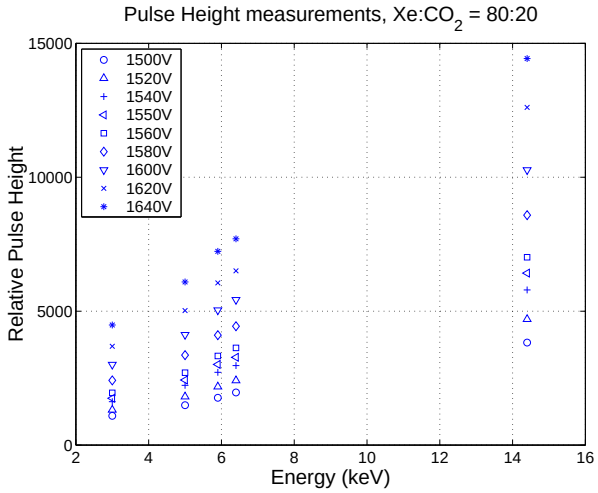

(b) Pulse height measurements vs. X-ray energy. Gain normalized to ^{55}Fe.

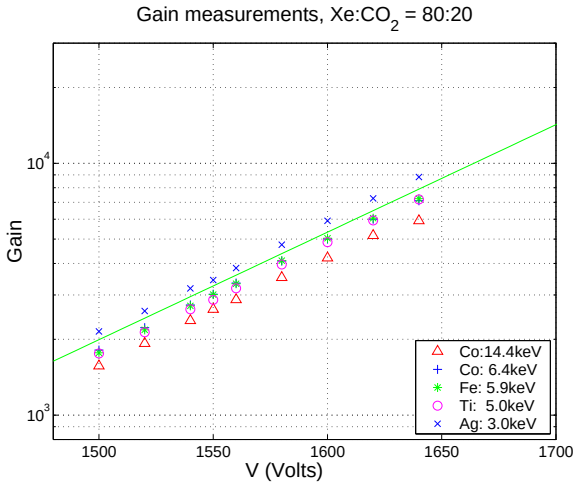

(c) Gain measurements vs. high voltage.

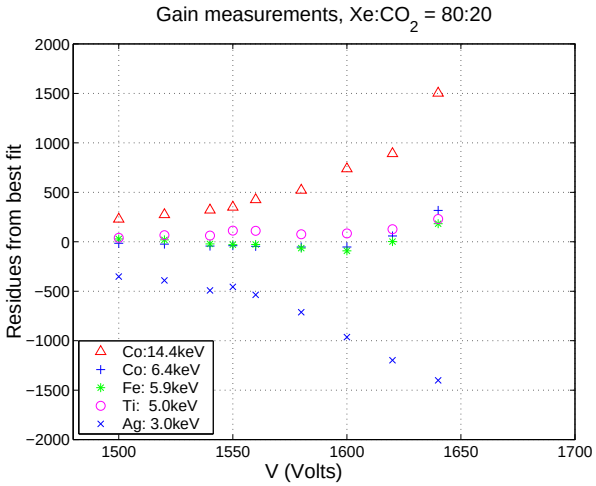

(d) Deviations in gain from the best fit.

Figure 4-5: Gain measurements using Xe:CO_2 = 80 : 20. Wire diameter of 30μm and tube diameter of 6mm.

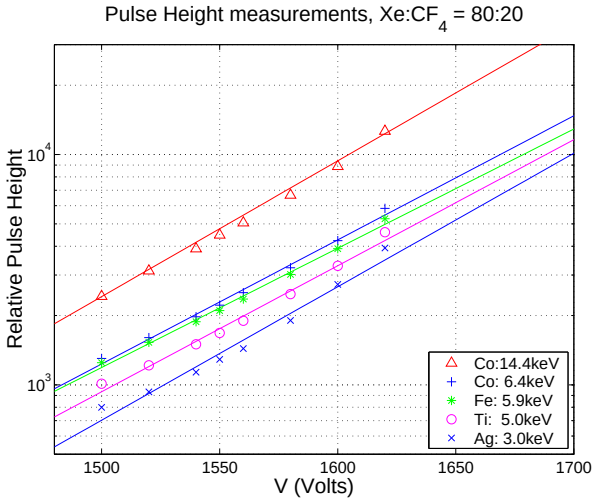

(a) Pulse height measurements vs. high voltage. Gain normalized to ^{55}Fe.

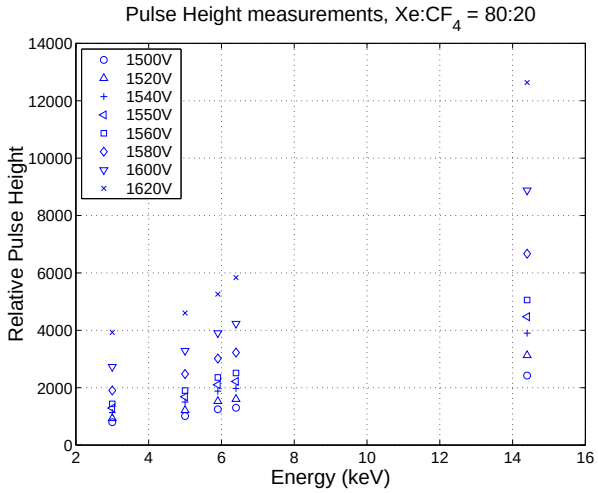

(b) Pulse height measurements vs. X-ray energy. Gain normalized to ^{55}Fe.

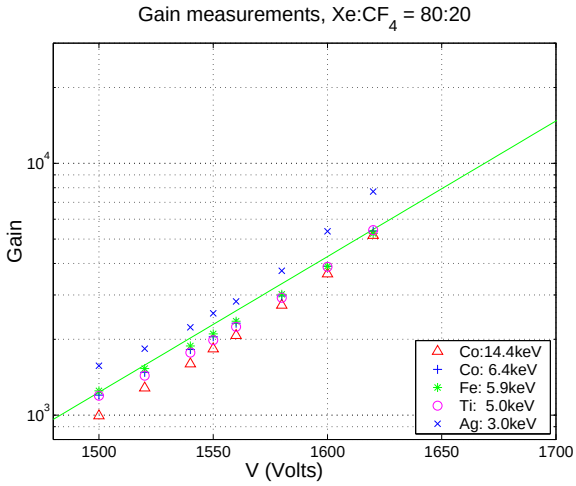

(c) Gain measurements vs. high voltage.

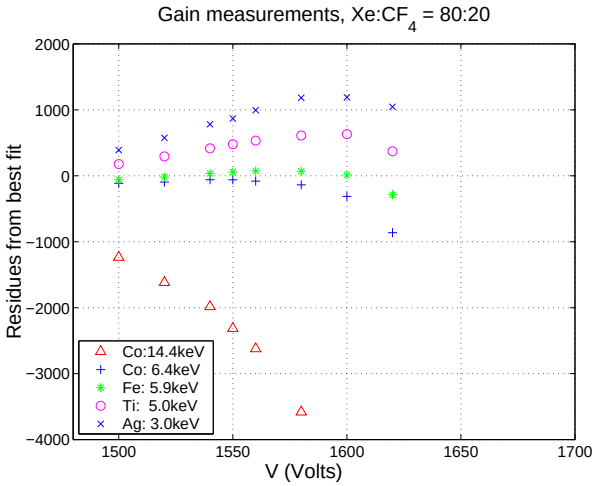

(d) Deviations in gain from the best fit.

Figure 4-6: Gain measurements using Xe:$CF_4 = 80 : 20$. Wire diameter of 30μm and tube diameter of 6mm.

4.3 Self-absorption

The material which generates TRD radiation also will absorb it. 20 mm radiator was chosen as a reasonable compromise, however the effects are large and must be measured. It is important to know the X-ray absorption constants due to the materials which the X-rays have to traverse before detection. The attenuation changes the energy spectrum and hence affects the e^+ and p separation. Attenuation properties of the walls of the detector and the radiator (polypropylene) have been measured and compared to closely related materials such as kapton and polyethylene.

If ρ is the density times the thickness of the material, which can also be thought of as the mass per area of a material, then

$$\frac{I}{I_o} = e^{(-\mu/\rho)} \tag{4.1}$$

where μ is the mass-energy attenuation constant and I and I_o are the final and initial intensities respectively.

The mass per area constant of materials used to determine the attenuation constants TRD per are shown in Table 4.2. All attenuation measurements were taken at a high voltage of 1550 and gain and geometry stability of the system was checked through channel #2.

Material	**Mass per area**
Kapton	0.0202 ± 0.0005 gr/cm^2
Straw tube	0.0080 ± 0.0013 gr/cm^2
Polyethylene	0.0187 ± 0.0003 gr/cm^2
Radiator	0.0270 ± 0.0005 gr/cm^2
Aluminum	0.00380 ± 0.00012 gr/cm^2

Table 4.2: Mass per area constants for materials used.

First, integral of counts around a particular X-ray peak was determined without any absorbers. Later, layers of materials were placed in between the source and straw tube #9. Count rate goes down as more and more layers are added. The ratio of counts with absorber to the original counts are plotted versus ρ, for each material as shown in Fig. 4-7. These measurements were performed with all 5 X-ray energies

and with the different materials listed, until the counting rate was too low. The absorption constant, μ was calculated by fitting to Eq. 4.1.

Radiator material is polypropylene and it is in chemical composition comparable to polyethylene, which is included in NIST tables. Kapton's chemical formula is $C_{22}H_{10}O_4N_2$. Since the attenuation constants scale with the chemical combination, it can be calculated. As shown in Fig. 4-9 and 4-8, the measurements agree reasonably with NIST data. These results will cross-check the already existing simulation calculation.

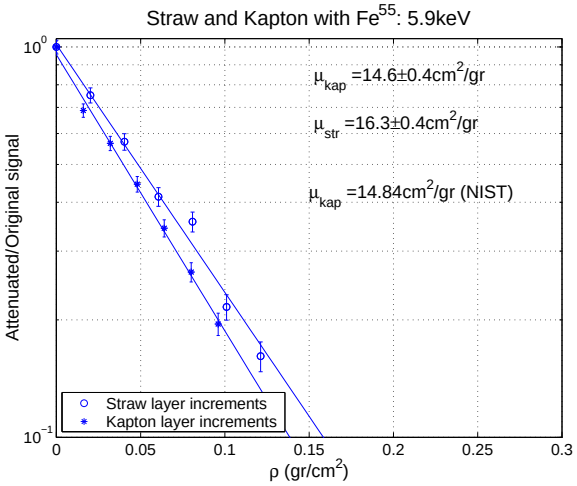

(a) Measurements with straw tube layers of thickness 72μm and kapton foils of thickness 0.12mm.

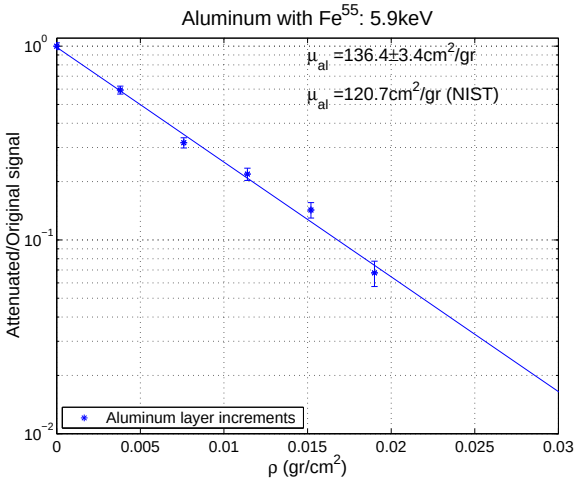

(b) Measurements with aluminum foils of thickness 12μm.

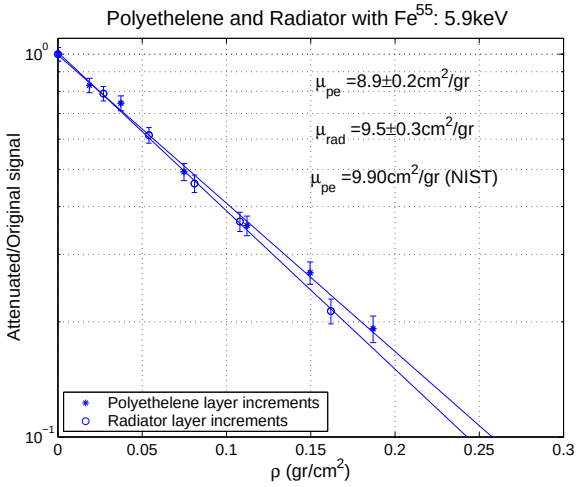

(c) Measurements with polyethylene foils of thickness 0.18mm and radiator layers of thickness 2cm.

Figure 4-7: Attenuation measurements with ^{55}Fe, compared to NIST data.

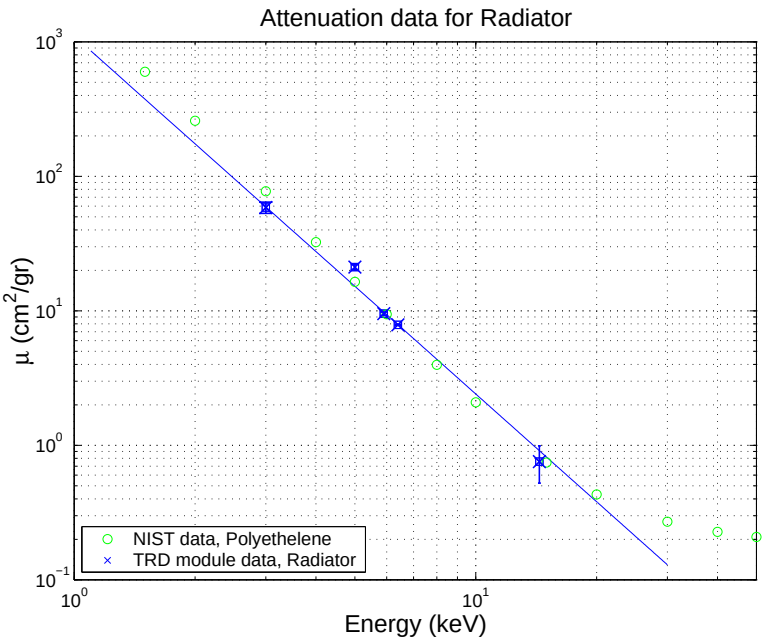

Figure 4-8: Energy dependence of measured attenuation constants for radiator material compared with theoretical calculations from NIST data for polyethylene

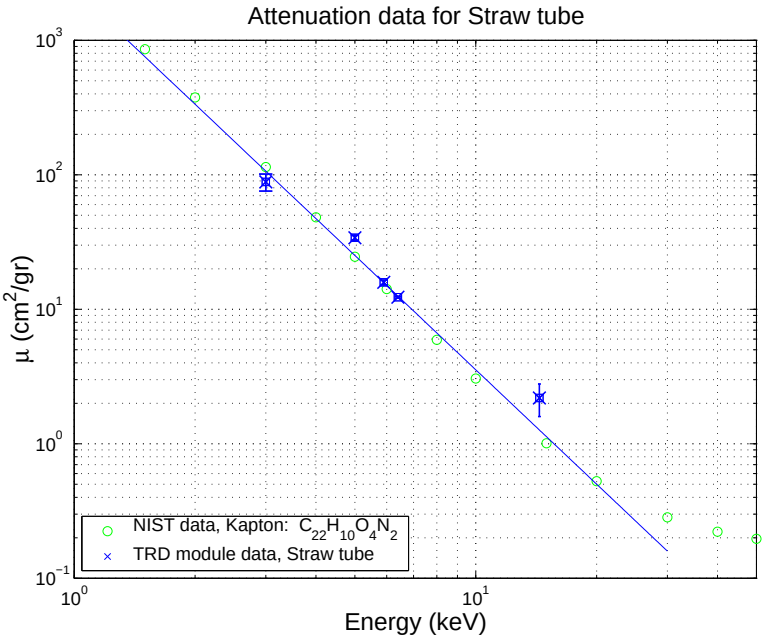

Figure 4-9: Energy dependence of measured attenuation constants for straw tube compared with theoretical calculations from NIST data for kapton

Chapter 5

Conclusion

5.1 Calculations

Using the attenuation constants obtained, we can calculate the TRD spectrum at different detector configurations in Fig. 5-1. The TRD spectrum with all X-ray absorption turned off can be obtained from the simulation. (Fig. 5-2)

First, lets take a simple approach and assume that this TRD spectrum is incident upon a straw tube or a radiator that is either creating and absorbing at the same time (C & A) or only absorbing (A). Then the percentages of photons that will pass through the material and not get absorbed are given on the Table 5.1.

Taking photons that are produced in Radiator-1, we can propogate them through the several material layers. As seen in 5-3, the lower energy X-rays are absorbed more than the high energy ones. Also seen in 5-4, many low energy X-rays are absorbed by the radiators and straw tubes before they can get to the Xenon. So effectively, the peak of the spectrum shifts towards higher energies. But, the high energy X-rays can penetrate the Xenon without getting detected. Integrating over the various

Material	**Mass per area**	**Survivors**
Radiator: C & A	0.12 gr/cm^2	21.6%
Radiator: A	0.12 gr/cm^2	10.2%
Straw tube	0.008 gr/cm^2	36.7%

Table 5.1: Survival probability of a photon in TRD material.

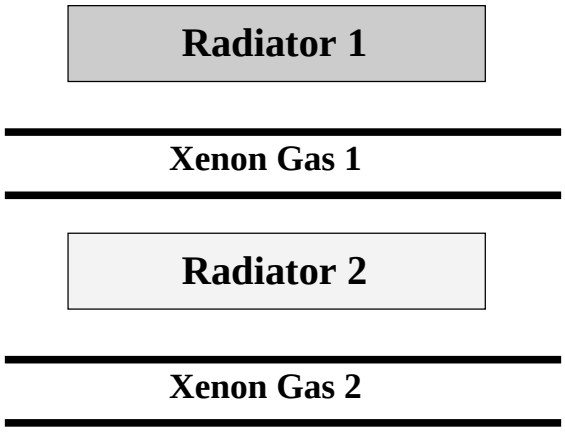

Figure 5-1: Passage of a photon through different TRD layers

Layer	Survivors
Start	100%
Before xenon layer-1	16.7%
After xenon layer-1	8.4%
Before xenon layer-2	4.4%
After xenon layer-2	3.2%

Table 5.2: Passage of a photon through different TRD layers.

energies of X-rays, the detection efficiency of photons in the first xenon filled TRD tube is found to be $8.3 \pm 0.5\%$ whereas the second TRD tube has an efficiency of only $1.2 \pm 0.1\%$ if the second radiator is only acting as an absorber.

The attenuation changed the TRD spectrum significantly as shown. This directly effects the positron-proton separation since as mentioned before protons do not produce TR photons below 1000 GeV. However, they deposit ionization loss energy into the tube just like the positrons do. The likelihood calculations have been carried out using spectrum from the simulation as in Fig. 5-5. At 50 GeV, there is 0.4% proton contamination in the positrons with 90% efficiency.

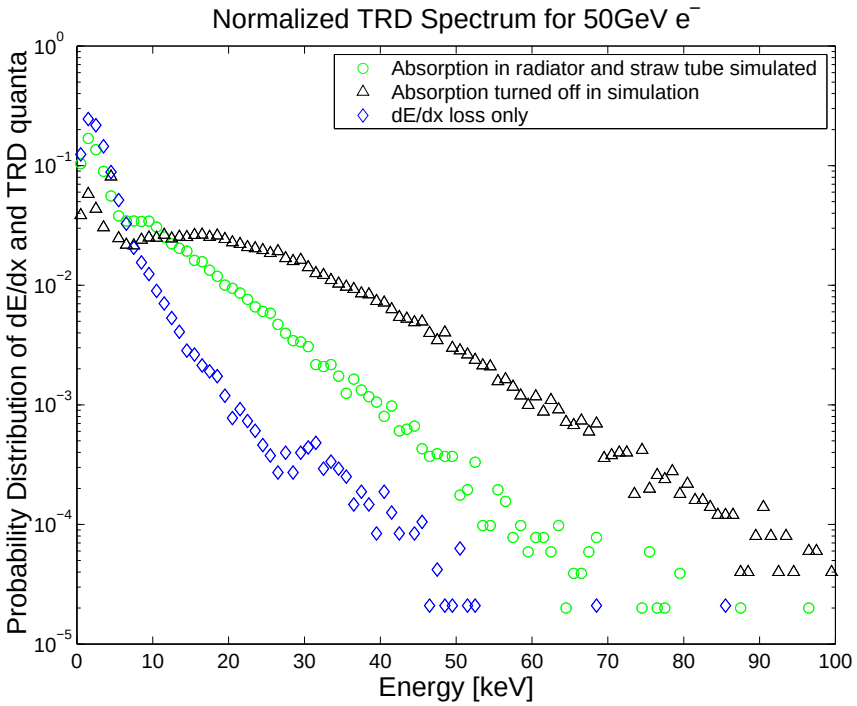

Figure 5-2: Calculated probability distribution of energy losses in 6mm Xe tubes of 50GeV electrons. Spectrum with TRD quanta ($\triangle$), attenuated in the straw tube and radiator material ($\circ$) and energy loss without TRD radiation($\Diamond$). All probabilities are normalized to 1.

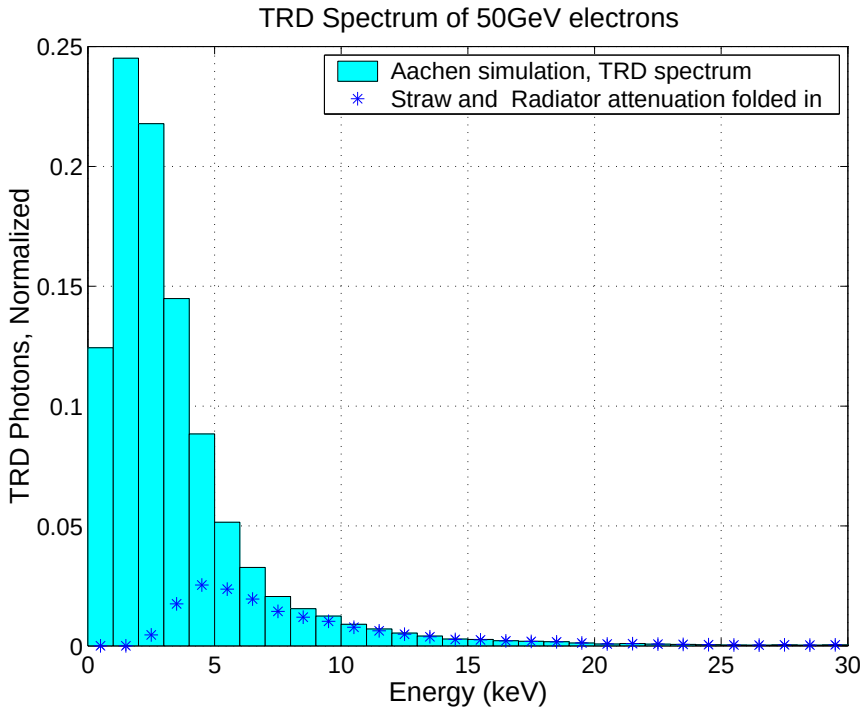

Figure 5-3: Histogram is the calculated probability distribution of TRD photons, normalized to 1 and the ($\star$)s are the surviving photons after accounting for the measured attenuation in the radiator and the straw tube.

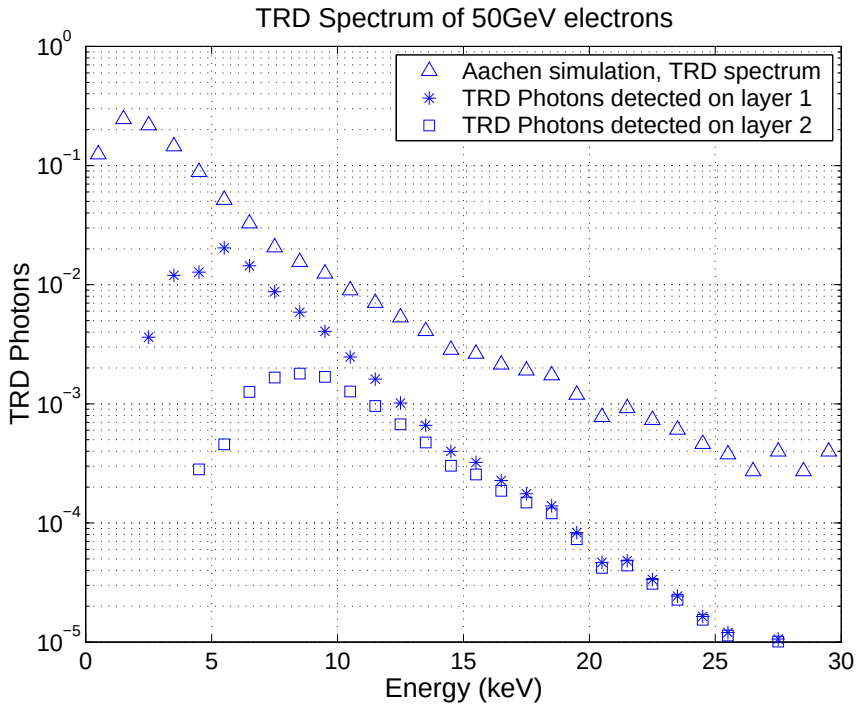

Figure 5-4: Detected photon spectra compared with produced spectra from theory.

5.2 Conclusion

Gas and gain studies for the AMS TRD were done. The feasibility of the two gas options was studied. The absorption constants of detector materials were measured and the effective absorptions were used to calculate the observed TRD spectra. The effect of attenuation on particle identification was discussed.

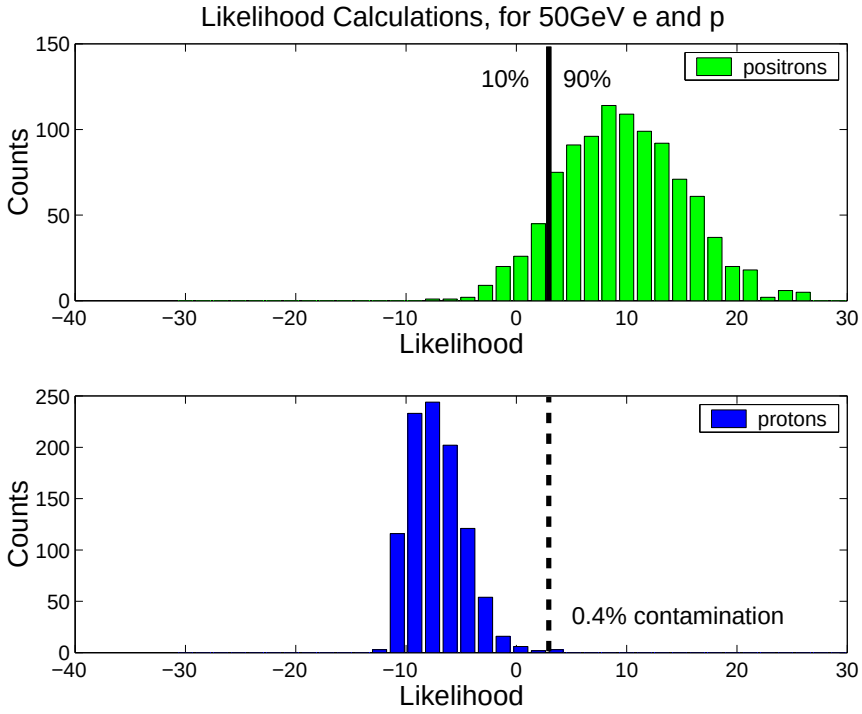

Figure 5-5: Likelihood functions for positron-proton separation.

Bibliography

[1] T. Akesson et al. Straw tube drift-time properties and electronics parameters for the ATLAS TRT detector. *Nucl. Instrum. Meth.*, A449:446–460, 2000.

[2] J. Alcaraz et al. Leptons in near earth orbit. *Phys. Lett.*, B484:10–22, 2000.

[3] J. Alcaraz et al. Protons in near earth orbit. *Phys. Lett.*, B472:215–226, 2000.

[4] M. Ambrosio et al. Measurement of the energy spectrum of underground muons at Gran Sasso with a transition radiation detector. *Astropart. Phys.*, 10:11–20, 1999.

[5] E. Barbarito et al. A high rejection transition radiation detector prototype to distinguish positrons from protons in a cosmic ray space laboratory. *Nucl. Instrum. Meth.*, A313:295–302, 1992.

[6] E. Barbarito et al. Straw chambers operating in vacuum for particle tracking and transition radiation detection in accelerator and space experiments. *Nucl. Instrum. Meth.*, A381:39–48, 1996.

[7] Aurelien Barrau. AMS: A particle observatory in space. 2001. eprint: astro-ph/0103493.

[8] G. Bassompierre et al. Performance of the NOMAD transition radiation detector. *Nucl. Instrum. Meth.*, A411:63–74, 1998.

[9] U. Becker et al. MIT LNS Gas R&D Home Page. 1999. URL: http://cyclotron.mit.edu/drift.

[10] R. Bellotti et al. A transition radiation detector for positron identification in particle astrophysics experiments. Presented at Int. Cosmic Ray Conf., Calgary, Canada, Jul 19- 30, 1993.

[11] W. Blum and L. Rolandi. *Particle Detection with Drift Chambers.* Springer-Verlag, Berlin, second edition, 1994. p. 1-38, 124-127.

[12] F. S. Cafagna. The PAMELA transition radiation detector. Prepared for 26th International Cosmic Ray Conference (ICRC 99), Salt Lake City, Utah, 17-25 Aug 1999.

[13] Application Software Group: Computing and Networks Division. *GEANT: Detector Description and Simulation Tool.* CERN Geneva, Switzerland, 1993. URL: http://wwwinfo.cern.ch/asdoc/geantold/GEANTMAIN.html.

[14] B. Dolgoshein. Transition radiation detectors. *Nucl. Instrum. Meth.*, A326:434–469, 1993.

[15] G. E. Graham et al. Design and test results of a transition radiation detector for a fermilab fixed target rare kaon decay experiment. *Nucl. Instrum. Meth.*, A367:224–227, 1995.

[16] D.E. Groom et al. Review of Particle Physics. *The European Physical Journal*, C15:163–178, 2000. URL: http://pdg.lbl.gov.

[17] J. H. Hubbell and S. M. Seltzer. Tables of X-Ray mass attenuation coefficients and mass-energy absorption coefficients, 1996. URL: http://physics.nist.gov/PhysRefData/XrayMassCoef/cover.html.

[18] J. D. Jackson. *Classical Electrodynamics.* John Wiley & Sons, Inc., New York, third edition, 1998. p. 646-654.

[19] W. R. Leo. *Techniques for Nuclear and Particle Physics Experiments.* Springer-Verlag, Berlin, first edition, 1987. p. 119-133.

[20] M. N. Mazziotta. Transition radiation detector in MACRO. 1999. eprint: hep-ex/9905018.

[21] Henryk Piekarz. Transition radiation detector in the D0 colliding beam experiment at Fermilab. Presented at 7th Vienna Wire Chamber Conference (WCC 95): Recent Trends and Alternative Techniques, Vienna, Austria, 13-17 Feb 1995.

[22] T. Sanuki et al. Precise measurement of cosmic-ray proton and helium spectra with the BESS spectrometer. *Astrophys. J.*, 545:1135, 2000.

[23] V. Saveliev. The HERA-B transition radiation detector. *Nucl. Instrum. Meth.*, A408:289–295, 1998.